THE JOURNAL OF BIOLOGICAL CHEMISTRY
Vol. 279, No. 12, Issue of March 19, pp. 11882–11889, 2004

Printed in U.S.A.

Structural Insights into Molecular Function of the Metastasis-associated Phosphatase PRL-3*

Received for publication, November 26, 2003, and in revised form, December 31, 2003
Published, JBC Papers in Press, January 1, 2004, DOI 10.1074/jbc.M312905200

Guennadi Kozlov‡, Jing Cheng§¶, Edmund Ziomek§, Denis Banville§, Kalle Gehring‡, and Irena Ekiel§¶‖

From the ‡Department of Biochemistry, McGill University, Montreal, Quebec H3G 1Y6, Canada, §Health Sector, Biotechnology Research Institute, National Research Council of Canada, Montreal, Quebec H4P 2R2, Canada, and the ¶Department of Chemistry and Biochemistry, Concordia University, Montreal, Quebec H3G 1M8, Canada

Phosphatases and kinases are the cellular signal transduction enzymes that control protein phosphorylation. PRL phosphatases constitute a novel class of small (20 kDa), prenylated phosphatases with oncogenic activity. In particular, PRL-3 is consistently overexpressed in liver metastasis in colorectal cancer cells and represents a new therapeutic target. Here, we present the solution structure of PRL-3, the first structure of a PRL phosphatase. The structure places PRL phosphatases in the class of dual specificity phosphatases with closest structural homology to the VHR phosphatase. The structure, coupled with kinetic studies of site-directed mutants, identifies functionally important residues and reveals unique features, differentiating PRLs from other phosphatases. These differences include an unusually hydrophobic active site without the catalytically important serine/threonine found in most other phosphatases. The position of the general acid loop indicates the presence of conformational change upon catalysis. The studies also identify a potential regulatory role of Cys^{49} that forms an intramolecular disulfide bond with the catalytic Cys^{104} even under mildly reducing conditions. Molecular modeling of the highly homologous PRL-1 and PRL-2 phosphatases revealed unique surface elements that are potentially important for specificity.

PRL (for phosphatase of regenerating liver) phosphatases constitute a novel class of small tyrosine phosphatases involved in the modulation of cell growth. Initial studies identified PRL-1 as an intermediate-early gene expressed in the early response of regenerating liver tissue to mitogens (1). Overexpression of this protein was shown to lead to cellular transformation (1–3). The biological role of PRL-1 is tissue-dependent. Its overexpression is associated with cell proliferation in the liver (1) but with differentiation of epithelial cells in the digestive system (4). The closely related phosphatases PRL-2 and PRL-3 are also involved in growth regulation, proliferation, and cell invasion (3, 5, 6). All three proteins are prenylated at their C terminus, which critically affects their cellular localization and function (6–8). As shown for the human PRL-2, the role of PRLs is associated with the regulation of progression through mitosis, and their cellular localization is likely controlled by the cell cycle (8).

PRL phosphatases are widely distributed in eukaryotes. In humans, PRL-1 and PRL-2 are ubiquitously expressed in various tissues (6), whereas PRL-3 is normally expressed in cardiac and skeletal muscles (5). Comprising typically only 140–180 amino acids, PRLs are among the smallest phosphatases. They consist of a single catalytic domain lacking any auxiliary docking/regulatory domains other than the prenylation site at the C terminus. PRLs contain the protein-tyrosine phosphatase (PTPase)[1] active consensus motif H*C*X*X*G*X*X*R*, referred to as the P-loop; however, their primary sequence shows only remote similarity to phosphatases in other regions. Tyrosine-specific phosphatases as well as dual specificity phosphatases (DSP), enzymes capable of dephosphorylating both phosphotyrosine and phosphothreonine/serine residues, share the same general catalytic mechanism. The key structural elements include the positively charged phosphate-binding region of the P-loop and a catalytic cysteine residue that possesses an unusually low pK_a of ~5 such that its side chain exists as a thiolate at a physiological pH. During catalysis, this cysteine acts as a nucleophile to form a thiophosphoryl enzyme intermediate, and a conserved aspartic acid in a neighboring loop participates in both the formation and the hydrolysis of the phosphoenzyme intermediate. The conserved arginine in the P-loop is important for the stabilization of the transition state (for a review, see Ref. 9). In many PTPases, correct positioning of the flexible loop containing the catalytic aspartate is critical for activation and catalytic performance of these enzymes (10).

Recent interest in PRL phosphatases relates to their role in cell proliferation, including promotion of cell migration, invasion, and metastasis (2–4, 7, 11, 12). SAGE (serial analysis of gene expression) experiments showed that PRL-3 is massively overexpressed in colon tumors metastasizing to the liver but not in nonmetastatic tumors and in normal colorectal epithelium (13). Further support for the involvement of PRL-3 in metastasis was provided by the finding of gene amplification in a significant fraction of metastatic lesions from different pa-

* This work was supported in part by funds from the Canadian Institutes of Health Research Grants 43954 (to I. E.) and 14219 (to K. G.). NANUC is funded by the Canadian Institutes of Health Research, the Natural Science and Engineering Research Council of Canada, and the University of Alberta. The costs of publication of this article were defrayed in part by the payment of page charges. This article must therefore be hereby marked "*advertisement*" in accordance with 18 U.S.C. Section 1734 solely to indicate this fact.

The atomic coordinates and structure factors (code 1R6H) have been deposited in the Protein Data Bank, Research Collaboratory for Structural Bioinformatics, Rutgers University, New Brunswick, NJ (http://www.rcsb.org/).

‖ To whom correspondence should be addressed. Tel.: 514-496-1041; Fax: 514-496-5143; E-mail: irena.ekiel@nrc.ca.

[1] The abbreviations used are: PTPase, protein-tyrosine phosphatase; DSP, dual specificity phosphatase; VHR, vaccinia H1-related phosphatase; CDC, cell division cycle phosphatase; KAP, kinase-associated phosphatase; NOE, nuclear Overhauser effect; NOESY, nuclear Overhauser effect correlation spectroscopy; DTT, dithiothreitol; OMFP, 3-*O*-methylfluorescein phosphate.

TABLE I
Structural statistics for PRL-3

Restraints for structure calculations	
Total restraints used	2320
Total NOE restraints	1969
Intraresidual	803
Sequential ($\|i - j\| = 1$)	371
Medium range ($1 < \|i - j\| < 5$)	301
Long range ($\|i - j\|$e5)	494
Hydrogen bond restraints	76
Dihedral angles restraints	275
Root mean square deviations from experimental restraints	
Distance deviations (Å)	0.018 ± 0.0007
Dihedral deviations (°)	0.940 ± 0.0306
Deviations from idealized geometry	
Bonds (Å)	0.0023 ± 0.0001
Angles (°)	0.4313 ± 0.0052
Impropers (°)	0.3897 ± 0.0091
Root mean square deviations of the 20 structures from the mean coordinates (Å)	
Backbone (residues Ala^{8}–Avg^{153})	0.49 ± 0.16
Heavy atoms (residues Ala^{8}–Avg^{153})	0.83 ± 0.13
Ramachandran plot statistics for residues Ala^{8}–Avg^{153} (%)	
Residues in most favored regions	87.42
Residues in additional allowed regions	11.62
Residues in generously allowed regions	0.12
Residues in disallowed regions	0.84

tients (13). Because of the massive levels of overexpression, PRL-3 constitutes a useful marker for metastasis and possibly a new therapeutic target. More studies at both the physiological and biochemical level are needed to better understand the function of PRL phosphatases and, in particular, to evaluate their involvement and role in metastasis.

Here, we determined the solution structure of PRL-3 and classify it as a member of the family of dual specificity phosphatases. The structure and site-directed mutagenesis experiments identify residues that are important for PRL-3 catalytic activity and reveal unique features that distinguish PRL-3 from other phosphatases.

EXPERIMENTAL PROCEDURES

PRL-3 Expression and Purification—The human phosphatase PRL-3 sequence, comprising amino acids 1–169, was subcloned into the pET15b vector (Novagen Inc., Madison, WI) and overexpressed in *Escherichia coli* BL21(DE3) as a His-tagged fusion protein. The protein was purified as described previously (14). The resulting protein contains the N-terminal extension (Gly-Ser-His) from the cleavage site of the vector and does not include the C-terminal prenylation site (Cys-Cys-Val-Met). Isotopically enriched PRL-3 was prepared from cells grown on minimal M9 medium containing [^{15}N]ammonium chloride with or without [$^{13}C_6$]glucose (Cambridge Isotopes Laboratory, Andover, MA). The PRL-3 isoforms were expressed and purified as described above.

PRL-3 mutants were obtained by site-directed mutagenesis using PCR. The identities of the proteins were checked by DNA sequencing and further verified at the protein level by mass spectrometry (Sciex APII electrospray mass spectrometer; Thornhill, ON, Canada). All of the mutants were expressed and purified using the same protocol as for the wild-type PRL-3.

NMR Spectroscopy—NMR samples with a protein concentration of 3 mM were exchanged into 50 mM phosphate buffer, 100 mM NaCl, 10–12 mM DTT, and 0.1 mM sodium azide, pH 6.80. NMR experiments were performed at 308 K. Backbone and side chain NMR signal assignments of PRL-3 were determined as described previously (14). NOE constraints for the structure determination were obtained from ^{15}N-edited and homonuclear NOESY obtained at Bruker DRX 500-MHz spectrometer and ^{13}C-edited NOESY acquired on a Varian Inova 800-MHz spectrometer. The mixing time was 110 ms for these experiments. $^{3}J_{H^N H^\alpha}$ coupling constants were obtained from an HNHA experiment (15). NMR spectra were processed using XWINNMR (Bruker Biospin) and GIFA (16) software and analyzed with XEASY (17).

Structure Calculations—NOE restraints were obtained from ^{15}N- and ^{13}C-edited three-dimensional NOESY experiments and from two-dimensional homonuclear NOESY spectra. The ϕ and ψ torsion angles were derived from C^α, C^β, and H^α chemical shifts using TALOS (18) and compared with experimental values resulting from an HNHA experiment. The structures were calculated using the ARIA module (19) implemented in the program CNS (version 1.1) (20). The initial set of several hundred NOEs was assigned for the protein and used to calculate the first ensemble of structures. Manually assigned distance constraints were classified according to the peak intensities as strong (1.8–3.0 Å), medium (1.8–4.0 Å), and weak (1.8–5.0 Å). Two-dimensional NOESY, three-dimensional ^{15}N NOESY, and three-dimensional ^{13}C NOESY spectra were used in the ARIA protocol to calibrate and assign NOE cross-peaks. The unambiguous distance restraints obtained after eight rounds of calculations were used to calculate the final set of structures. The quality of the obtained structures was assessed using PROCHECK (21). The statistics for the structure calculations are shown in Table I. The coordinates have been deposited with the Protein Data Bank (code 1R6H), and the chemical shift assignments have been deposited with the BioMagResBank (accession number 5455).

Enzymatic Assays—Enzymatic assays were carried out with 3-*O*-methylfluorescein phosphate (OMFP) as a substrate using absorbance at 450 nm for detection of the product (22). All of the assays were performed at 22 °C in TBA buffer (40 mM Tris-HCl, 150 mM NaCl, pH 6.15), containing 6 mM DTT, 5% Me_2SO. The substrate concentration ranged from 0 to 200 μM. Enzyme concentrations for the wild-type protein and the D71A and C49A mutants were determined from the "burst" amplitude (B) as 2.1, 4.5, and 2.5 μM, respectively. Concentration of the A111S mutant was calculated to be 0.5 μM. Hydrolysis was initiated by the addition of the enzyme to the reaction mixture and monitored for 90 min using a SpectraMAX-220 (Molecular Devices, Sunnyvale, CA) plate reader.

The raw data were fitted to Equation 1,

$$v = [(V_0 \times t) + (V_0 - V_s/k) \times (1 - e^{-kt})] + a \qquad \text{(Eq. 1)}$$

where V_0 is the initial rate, k is the reaction constant (burst constant), and V_s is the steady-state rate for the linear portion of the reaction plot. The burst amplitude (B) can be obtained by intersecting the linear part of the reaction plot with the y axis (product). The B value derived from the plot for the reaction where [S] $\gg K_m$, *i.e.* saturating substrate concentration, is stoichiometric to the enzyme concentration [E].

The kinetic constants were defined according to the following enzymatic scheme,

$$E + S \underset{k_{-1}}{\overset{k_1}{\rightleftharpoons}} ES \xrightarrow{k_2} E\cdots P \xrightarrow{k_3} E + P$$

SCHEME 1

where E is the enzyme, S is the substrate, ES is the enzyme-substrate complex, $E\cdots P$ is the phosphoenzyme intermediate, and P is the leaving phosphate group. The Michaelis-Menten equation was used to obtain k_{cat} and K_m after fitting V_s *versus* [S]. To analyze the exponential phase of the progress curve and to obtain $k_2 + k_3$ and K_S values k_{burst} (burst constant) was fitted against [S] to provide Equation 2.

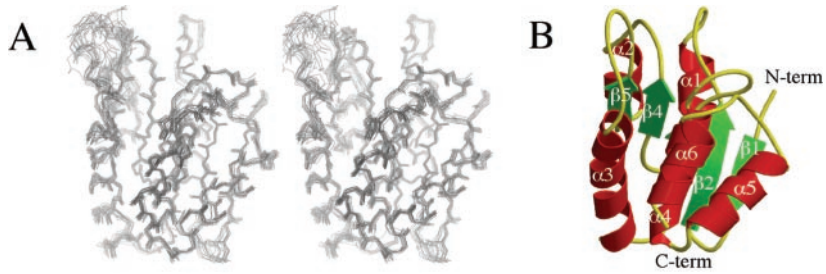

FIG. 1. **Structure of PRL-3.** *A*, stereo view of the backbone superposition of the 20 lowest energy structures for residues Ala[8]–Gln[156]. The unstructured N and C termini are not shown. *B*, ribbon representation of the average PRL-3 structure generated with MOLSCRIPT (41) and Raster3D (42). The secondary structure elements and N and C termini are labeled.

$$k_{burst} = (k_2 + k_3) \times [S]/(K_S + [S]) \quad \text{(Eq. 2)}$$

To dissect $k_2 + k_3$ sum of the rate constants, k_2 was derived after fitting *B versus* [S] to Equation 3.

$$B = [E](k_2/(k_2 + k_3))^2/(1 + (K_m/[S]))^2 \quad \text{(Eq. 3)}$$

When $k_2 \gg k_3$, *i.e.* dissociation of the $E \cdots P$ to $E + P$ is rate-limiting, $k_3 = k_{cat}$, and k_{cat}/K_m represents the catalytic efficiency of the phosphatase (22).

Molecular Modeling—Three-dimensional models of phosphatases PRL-1 and PRL-2 were constructed by homology modeling using the program Modeler 6v1 (23), using the experimentally determined structure of PRL-3 as a template. Sybyl 6.4 software (Tripos, St. Louis, MO) was used for further structure refinement and analysis. Structural refinement was performed by energy minimization using an AMBER 4.1 all-atom force field (24) with the Powell minimizer, a distance-dependent (4r) dielectric constant and an 8 Å nonbonded cut-off. The N and C termini were blocked with acetyl- and methylamino groups, respectively, and hydrogen atoms were added explicitly.

RESULTS

Solution Structure of PRL-3—We determined the structure of the human phosphatase PRL-3, the first of the PRL protein family. The previously reported resonance assignments (14) were used to assign NOEs from heteronuclear ^{15}N- and ^{13}C-edited three-dimensional NOESY and homonuclear two-dimensional NOESY experiments. The excellent quality spectra yielded a large number of distance constraints. TALOS was applied to generate dihedral angle constraints based on C^α, C^β, and H^α chemical shifts. These values were confirmed by experimentally determined coupling constants from an HNHA experiment. On average, 15.4 constraints/residue in the PRL-3 structured region (Ala[8]–Arg[153]) were used to calculate the PRL-3 structure. The 20 lowest energy structures out of 60 calculated were chosen to represent the final ensemble. The structural statistics are shown in Table I.

PRL-3 is comprised of a five-stranded β-sheet and six α-helices (Fig. 1). Strand β1 (Val[10]–Ser[13]) is antiparallel with respect to the remaining four parallel strands β2 (Met[17]–Thr[22]), β3 (Val[45]–Val[48]), β4 (Val[65]–Trp[68]), and β5 (Cys[99]–Val[102]). The helices α1 (Leu[30]–Tyr[40]) and α2 (Lys[55]–Asp[61]) are on one side of the β-sheet, and the remaining four, α3 (Lys[79]–Glu[94]), α4 (Ala[111]–Ser[122]), α5 (Lys[125]–Gln[135]), and α6 (Lys[144]–Tyr[152]), form a cluster on the opposite side of the β-sheet.

This arrangement of the secondary structure elements and overall fold is typical for DSP, structurally classifying PRL-3 as a member of this class of phosphatases. A comparison using DALI server reveals the closest similarity to the dual specificity phosphatases VHR (Protein Data Bank code 1vhr), PTEN (the phosphatase and tensin homologue; 1d5r), and KAP (1fpz) with Z scores of 10.4, 10.1, and 9.9, respectively. The root mean square deviation value between PRL-3 and each phosphatase is ~2 Å for the 60–80 α-carbons in the conserved elements of secondary structure. Structure-based sequence alignment with other dual specificity phosphatases and tyrosine phosphatases shows sequence identity below 20%, which is typical for this relatively divergent class of enzymes (Fig. 2).

This low sequence similarity leads to significant local structural differences. Interestingly, particularly large differences are observed in the loops surrounding the active site, responsible for both catalytic activity and substrate specificity. Fig. 3*A* shows an enlarged view of this region in PRL-3. The catalytic residues Cys[104] and Arg[110] are located at opposite ends of the catalytic P-loop. The hydrophobicity of conserved amino acids between Cys[104] and Arg[110] distinguishes PRL-3 from other dual specificity phosphatases. The amino acids in this region have been shown to contribute to substrate specificity for numerous phosphatases (25, 26). The other distinct feature of the PRL-3 catalytic site is the lack of protruding loops (Fig. 3*B*), which often participate in substrate binding (10, 27). The N terminus, preceding strand β1, which is usually structured in protein-tyrosine phosphatases and contributes to substrate binding, is unstructured and mobile in PRL-3. The region following strand β2, which recognizes binding partners for KAP phosphatase (27), is much shorter and flat. The loop following strand β3 is also much shorter and flatter than in the PTP1B, VHR, PYST, and KAP phosphatases (10, 27, 28). The resulting catalytic pocket is extremely shallow and suggests a broad range of specificity for PRL-3.

Dephosphorylation is mediated by an acidic residue in the loop adjacent to the catalytic P-loop that serves as a general acid by contributing a proton to the leaving phenolate or serine/threonine group (29). Sequence alignments suggest that Asp[72] in the β4-α3 loop could serve as a general acid for PRL-3 (Fig. 2). This loop also includes four prolines and two glycines responsible for its unusual conformation and high mobility (data not shown). This loop does not seem to interact with other parts of the protein and may undergo conformational changes upon substrate binding. Such substrate-induced conformational adjustment was observed for PTP1B and PYST (10, 30). It is possible that PRL-3 requires substrate activation, bringing the general acid residue closer to the catalytic cysteine to become fully active because poor activity was observed with synthetic substrates (see below).

Mutagenesis and Kinetic Analysis—The conserved catalytic residues Cys[104] and Arg[110] define the signature motif of PTPases and suggest a similar mechanism of dephosphorylation in PRL phosphatases. Because the C104A mutation was already shown to abolish the catalytic activity of PRL-3 (5), our mutagenesis experiments focused on the other conserved residues of the active site such as Ala[111], Asp[71], Asp[72], and Cys[49].

PRL-3 showed extremely low activity with phosphorylated peptides and the commonly used synthetic substrate, *p*-nitrophenyl phosphate (data not shown). For this reason, a more reactive substrate, OMFP, was chosen (22). Kinetic analysis of the wild-type protein showed a slow, two-step reaction with the formation of the phosphoenzyme intermediate and very slow, kinetically limiting release of phosphate group for regeneration of the free enzyme (Fig. 4). This differs from the fast burst phase of catalysis observed with other phosphatases (22, 31).

The rate-limiting step for PRL-3 activity is the dephosphorylation (regeneration) of the enzyme. The value of k_{cat}/K_m obtained for the wild-type PRL-3 was 7.5 s^{-1} M^{-1}, which is 3 orders of magnitude lower than that for a typical DSP such as

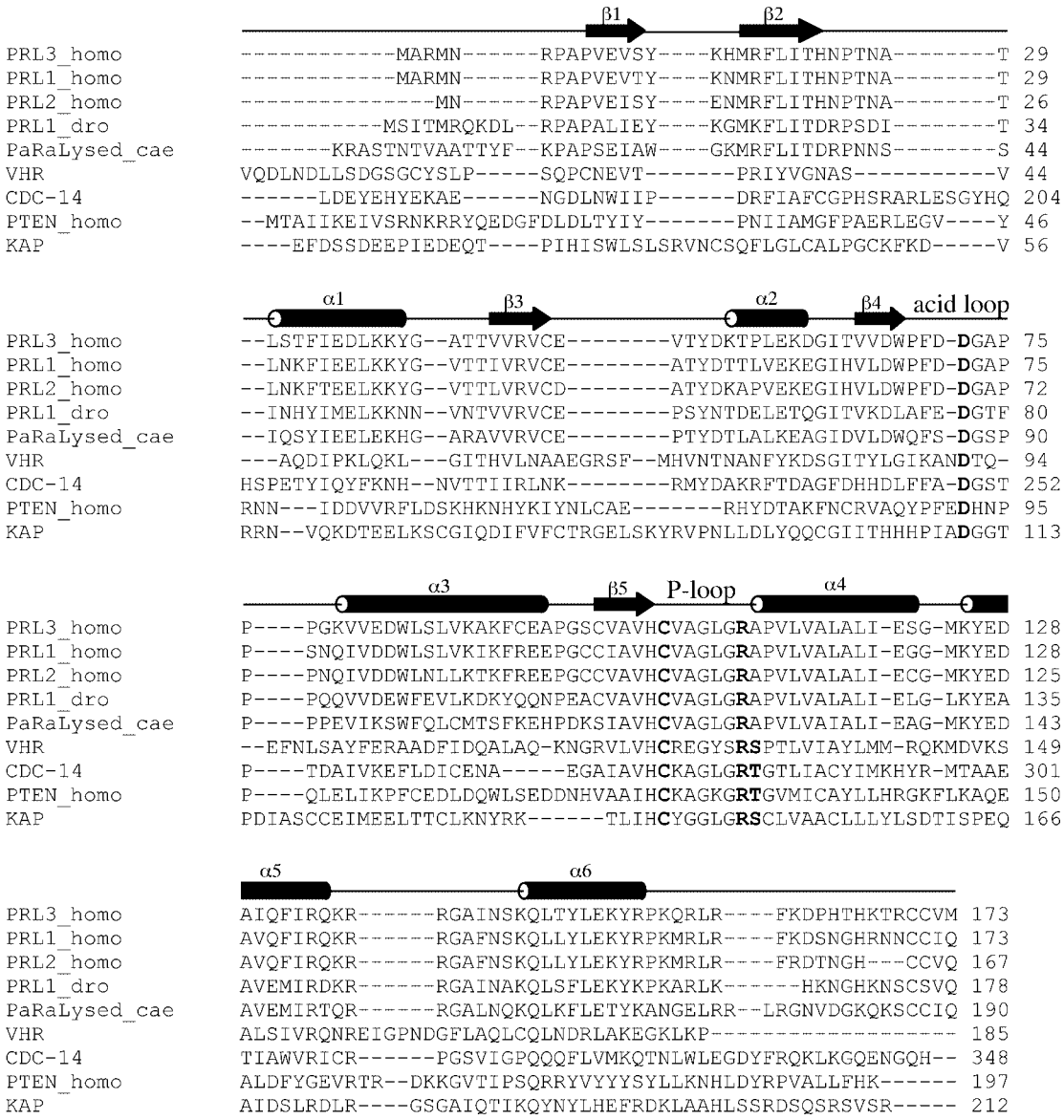

FIG. 2. **PRL phosphatases are highly homologous within their family but show low sequence similarity to the catalytic domains of other dual specificity phosphatases.** The aligned phosphatases include human PRL-3 (gi:14589856), PRL-1 (gi:4506283), PRL-2 (gi:4506285), *Drosophila* PRL-1 (gi:3135665), worm PaRaLysed_cae (gi:17569857), human VHR (gi:181840), CDC14 (gi:34811075), PTEN (gi:1916328), and KAP (gi:443669). The secondary structural elements refer to PRL-3. The catalytic residues are shown in *bold type*.

CDC25 and VHR (22). Surprisingly, both constants K_S and K_m (Table II) are very similar to those determined for CDC25 (23), implying that in the case of PRL-3 not substrate binding but stability of the phosphoenzyme (EP) is responsible for the slow kinetics.

A111S Mutant—The most striking feature in the catalytic site of PRL-3 is the presence of an alanine next to the catalytic arginine in the P-loop. Nearly all tyrosine and dual specificity phosphatases have a serine or threonine in this position, and the hydroxyl group of this conserved residue is important for the breakdown of the phosphoenzyme intermediate and for stabilizing the thiolate group of the catalytic cysteine (31, 32). The alanine to serine mutation significantly improves both the burst rate and the dephosphorylation efficiency (Fig. 4 and Table II). Under the experimental conditions used in this paper, it was possible to monitor only the steady-state portion of the kinetic curve for the A111S mutant. However, the size of the burst phase can be measured from the non-zero *y* intercept in the kinetic curve of Fig. 4. Increasing the enzyme concentration from 0.5 to 2.5 μM linearly increased the size of the burst. The amplitude also showed substrate concentration dependence at concentrations below saturation (~100 μM). These results suggest that the A111S mutant follows two-phase kinetics but with a more rapid burst phase similar to that of CDC25 and VHR. Despite the improvement in catalytic performance of the A111S mutant, the k_{cat} remained 2 orders of the magnitude lower than the same constant for VHR phosphatase (22). It appears that the presence of Ala^{111} in the catalytic site of PRL-3 only partially explains the very low catalytic efficiency.

D71A and D72A Mutants—One of the two aspartic acids Asp^{71} and Asp^{72} is expected to act as a general acid in the catalysis (Fig. 2). The D72A mutation lowered the k_{cat} value to a level where it could not be measured with our experimental setup, confirming its catalytic role. On the other hand, the D71A mutant had a k_{cat}/K_m value similar to that of wild-type PRL-3, indicating that Asp^{71} plays no role in catalysis.

C49A Mutant—The PRL-3 structure reveals the presence of Cys^{49} in close vicinity to the catalytic Cys^{104}. The disulfide bond formation between these cysteines provides another plau-

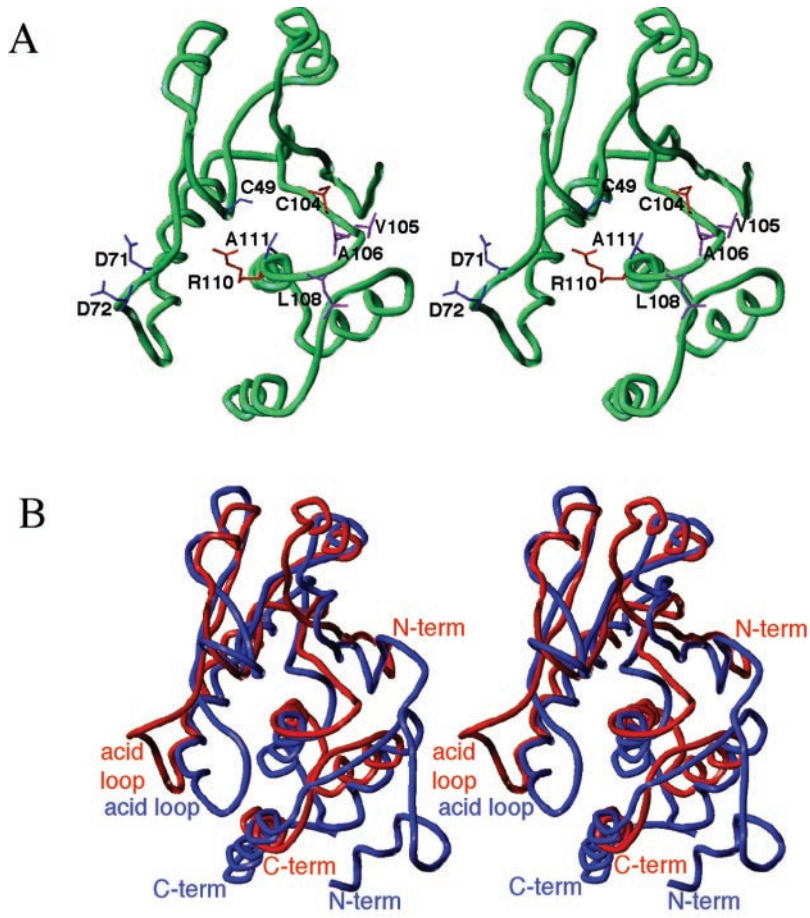

FIG. 3. **The positioning of the loops around the catalytic site differentiates PRL-3 from other dual specificity phosphatases.** *A*, stereo view of the catalytic site of PRL-3 shows the requirement for activation to bring the general acid Asp^{72} closer to the catalytic Cys^{104}. The catalytic residues are shown in *red*. The residues for which mutagenesis was done are colored in *blue*. *B*, stereo view of backbone superposition of PRL-3 (in *red*) and VHR phosphatase (Protein Data Bank code 1VHR; *blue*), which is based on 74 C^{α} atoms from secondary structure elements. Significant differences in the vicinity of the catalytic site reflect a different substrate specificity for these enzymes. The critical loops for substrate recognition are labeled. *N-term* , N terminus; *C-term*, C terminus.

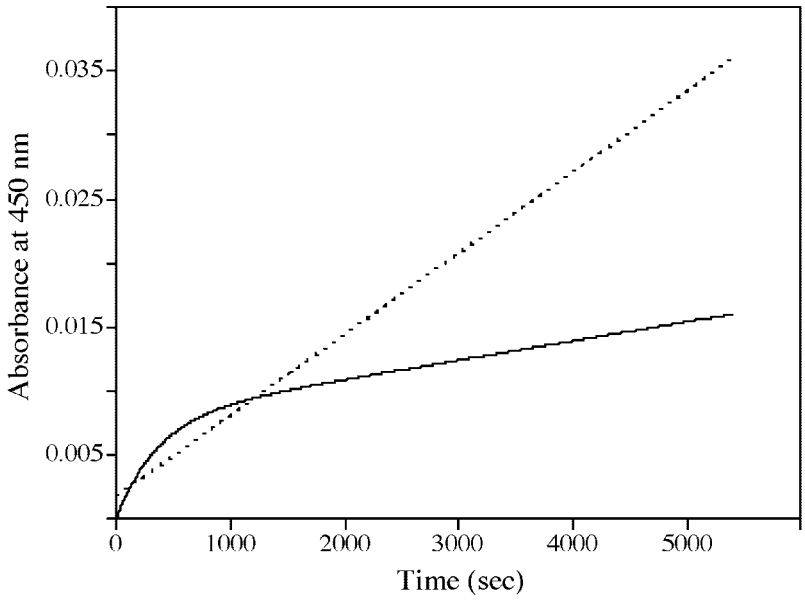

FIG. 4. **The kinetic curves showing hydrolysis of OMFP by the wild-type PRL-3 (*solid line*) and the A111S mutant (*dotted line*) monitored using absorbance at 450 nm.** The A111S mutation improves catalytic efficiency and shortens the first step of the two-step reaction, which is demonstrated by the wild-type protein. The reaction was initiated by adding 2.1μM wild-type PRL-3 (*solid line*) and 0.5 μM A111S mutant (*dotted line*) to the reaction mixture composed of 40 mM Tris-HCl, 150 mM NaCl pH 6.15, 6 mM DTT, 5% Me_2SO, and 100 μM OMFP. Intersection of the A111S progress curve with the *y* axis corresponds well to the calculated concentration of the enzyme.

sible explanation for the observed low catalytic activity. This is particularly important because a similar intramolecular disulfide bond in KAP phosphatase was extremely stable, even in the presence of 0.2 M DTT (27). Mutation of the noncatalytic cysteine residue in KAP prevented the formation of this disulfide bond and increased the enzymatic activity 40-fold. In PRL-3, the kinetics of the C49A mutant was identical to that of the wild-type protein, indicating that Cys^{49} is not responsible for the low enzymatic activity of PRL-3.

Oxidation of the Catalytic Cysteine—Under less strongly reducing conditions than used for the kinetic studies, disulfide bond formation between Cys^{49} and Cys^{104} could be detected by NMR and gel electrophoresis. Fig. 5 shows a fragment of a ^{1}H-^{15}N heteronuclear single-quantum correlation spectra of ^{15}N-enriched PRL-3 under mildly (0.5 mM DTT; Fig. 5*A*) and strongly (15 mM DTT; Fig. 5B) reducing conditions. Two species are present in the first spectrum (Fig. 5*A*), corresponding to a mixture of the reduced and oxidized forms of PRL-3. The oxidized form disappears as DTT is added, and only the reduced form is detected at a high concentration of DTT (Fig. 5*B*). Gel

TABLE II
Results of kinetic analysis for the wild-type PRL-3 and the PRL-3 mutants

PRL-3	Exponential phase[a]		Steady-state phase			
	k_2	K_S	k_{cat}	K_m	Relative k_{cat}	Relative k_{cat}/K_m[b]
	s^{-1}	μM	s^{-1}	μM		
Wild type	$9.8 \cdot 10^{-3}$	389.0	$2.5 \cdot 10^{-4}$	34.4	1.0	1.0
C49A	$4.5 \cdot 10^{-3}$	330.0	$2.7 \cdot 10^{-4}$	38.7	1.1	0.9
D71A	$3.2 \cdot 10^{-3}$	99.8	$1.7 \cdot 10^{-4}$	81.4	0.7	0.3
D72A			$<1.0 \cdot 10^{-5}$			
A111S	ND[c]	ND	$7.1 \cdot 10^{-3}$	111.0	28.4	8.6

[a] The analysis of the "burst" phase showed that $k_2 + k_3 = k_2$, indicating that $k_2 \gg k_3$.
[b] The k_{cat}/K_m for wild-type PRL-3 is 7.5 s^{-1} M^{-1}.
[c] ND, not determined.

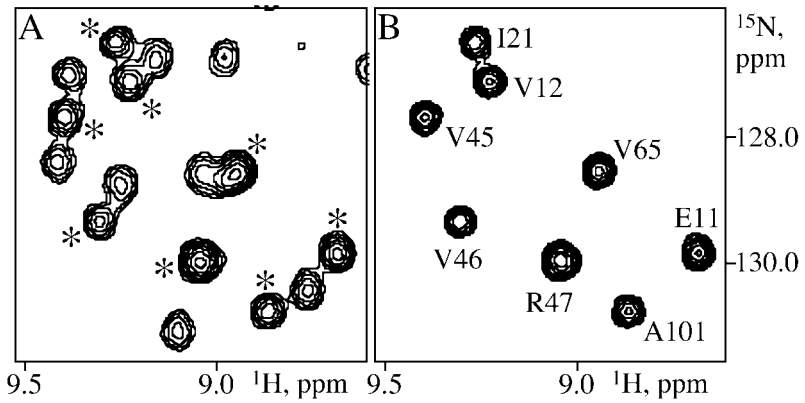

FIG. 5. **Reversible oxidation of PRL-3 monitored by NMR spectroscopy.** Two-dimensional spectra of ^{15}N-enriched PRL-3 in the NMR buffer containing 0.5 mM (*A*) and 15 mM (*B*) DTT. The residues are labeled for the reduced form of PRL-3 in *B*, and the corresponding peaks in the partially oxidized form are marked with *asterisks* in *A*.

electrophoresis can also be used to monitor the oxidation of phosphatases because the reduced and oxidized forms have different electrophoretic mobilities (33, 34). Characterization of the wild-type PRL-3 by gel electrophoresis showed two bands corresponding to the oxidized and reduced forms (data not shown). The C49A mutant produced a single band, confirming that Cys^{49} is involved in disulfide bond formation. These results indicate that PRL-3 is capable of forming an intramolecular disulfide between Cys^{49} and the catalytic Cys^{104} in a similar fashion to PTEN and CDC25 (33, 34).

Isoforms of PRL-3—Two alternative splicing variants of PRL-3 have the Glu^{11}–Ile^{34} fragment[2] or the Ala^{111}–Gln^{135} fragment (gi:13111875) deleted. Analysis of the PRL-3 structure indicates that these deletions would eliminate folded regions from strands β1–β3 in the first isoform and the two helices α4 and α5 in the second. Interestingly, the ends of the deletions map to neighboring loops, which raised the intriguing possibility that the isoforms are structurally reduced versions of the dual specificity phosphatase fold. To investigate this, isoforms 2 and 3 of PRL-3 were expressed and analyzed by NMR and enzymatic assays. Both isoforms were unstructured and inactive, demonstrating that the deletions compromised the structural integrity of PRL-3, causing unfolding and a loss of activity. Although the *in vivo* expression of the shorter PRL-3 isoforms is yet to be confirmed, our results demonstrate that only the full-length PRL-3 is biologically active.

Molecular Models of PRL-1 and PRL-2—To address the differences in biological roles of PRLs, molecular modeling was used to generate models for the human PRL-1 and PRL-2 phosphatases based on their high sequence similarity to PRL-3 (83 and 78% amino acid identity). All three phosphatases display striking conservation of amino acids around the P-loop (Fig. 6, *A* and *B*). The only variable amino acid in the vicinity of the active site that can potentially contribute to substrate specificity is Ile^{141} in PRL-3, which is phenylalanine in both PRL-1 and PRL-2. Nearly all amino acids, which are different in PRL-1, -2, and -3, cluster on the face opposite the active site. Fig. 6*C* shows the conserved residues in PRL phosphatases from a wide range of eukaryotes. This analysis reveals that the most highly conserved regions are in the immediate vicinity of the catalytic site along with a small number conserved, surface-exposed amino acids in other regions.

[2] D. Banville, unpublished results.

DISCUSSION

PRLs are a distinct class of small phosphatases within the family of DSP. They consist of a catalytic domain and a unique C-terminal prenylation site that is necessary for their cellular localization (7, 8). The family of DSPs shares a low sequence similarity, but PRL phosphatases are closely related, displaying over 40% sequence identity between lower eukaryotes and human and above 70% among mammals. Nearly all of the conserved amino acids have either a clear structural role or are part of the active site (Fig. 6). The first group includes residues from the hydrophobic core and numerous prolines and glycines in loops between elements of the secondary structure. The conserved catalytic regions, which participate in substrate binding and confer specificity, include the P-loop, the Asp^{72}-containing general acid loop, and the α5-α6 loop. The particularly strong sequence conservation around the catalytic site suggests a similar substrate specificity in PRLs. Two unique features of the P-loop should affect the catalytic mechanism and specificity of PRL phosphatases. First, the highly conserved amino acids Val^{105}-Ala-Gly-Leu-Gly^{109} define the hydrophobic character of the P-loop and may indicate a preference for more hydrophobic substrates than those of other phosphatases. Second, the C-terminal sequence of the P-loop is very unusual, Ala^{111}-Pro^{112}-Val^{113}, and the proline residue likely provides a unique conformational restrain in this critical position.

PRL-3 does not have the N-terminal substrate recognition region, which is responsible for the phosphotyrosine specificity in PTP1B. Because of the unique flat conformation of the loops

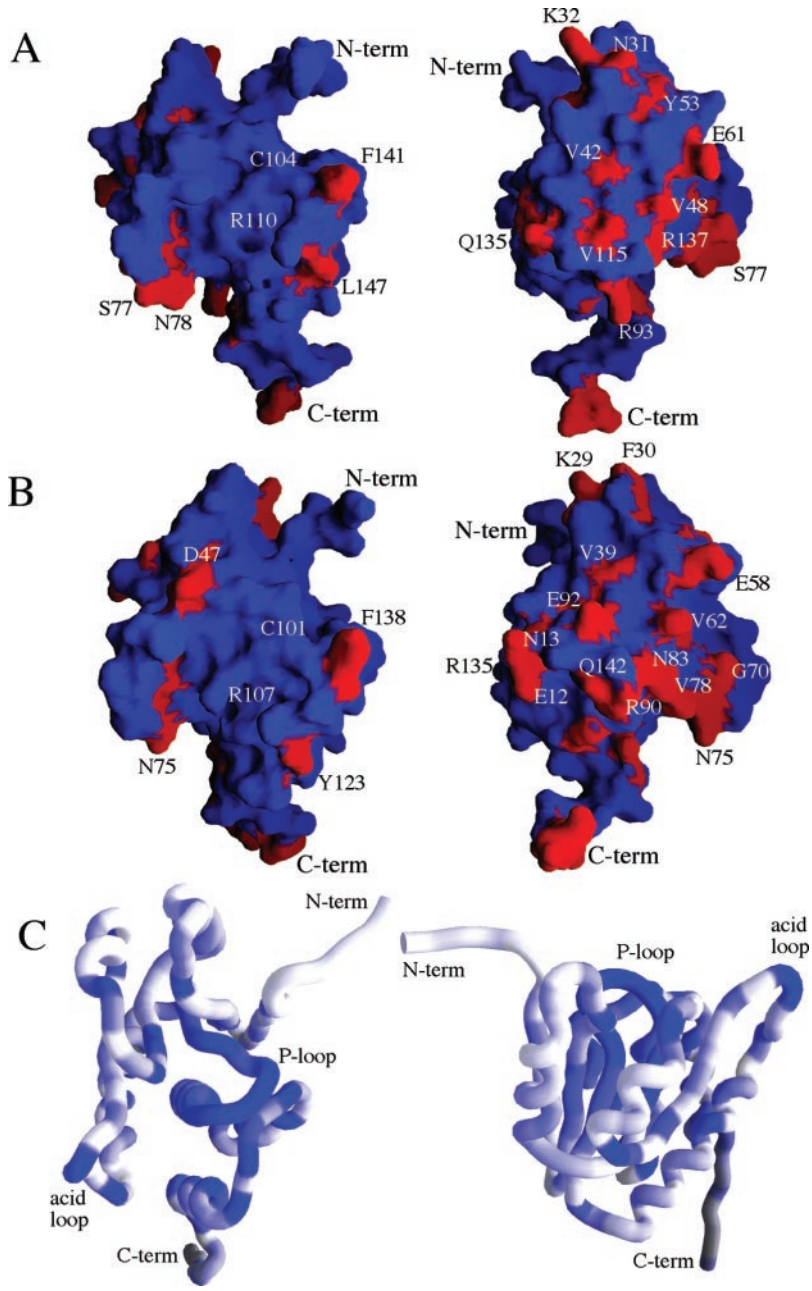

FIG. 6. **Sequence similarity analysis of PRL phosphatases shows highest conservation of residues in the active site.** The amino acids in the molecular models of human phosphatases PRL-1 (*A*) and PRL-2 (*B*) that are different than those in PRL-3 are colored in *red*. The catalytic residues in the P-loop and amino acids different from PRL-3 are labeled. Two orientations of each phosphatase are shown. *C*, C^{α} trace of PRL-3 is color-coded according to the phylogenetic conservation among 55 PRL phosphatases. An increase in sequence identity corresponds to the change in color from *white* to *blue*. The catalytic P-loop and general acid loop are labeled. The figures were generated with GRASP (43).

surrounding the catalytic P-loop, the catalytic cleft of PRL-3 is the shallowest of all known phosphatases. The structure of the complex between KAP and phospho-CDK2 showed that, unlike tyrosine phosphatases, the substrate specificity of DSPs may rely on interactions distant from the active site of the catalytic domain (27). These interactions may also involve various loops, surrounding the catalytic P-loop. The loop between the two C-terminal helices α5 and α6 of PRL-3 is positioned similarly to the corresponding loop in the KAP structure and likewise may play a role in substrate recognition. On the contrary, the unique KAP antiparallel β-hairpin with the key Lys^{54} at its tip that participates in substrate binding has no structural equivalent in PRL-3. Although sequence alignments suggest that CDC14 is the closest homologue, structural comparison shows that PRLs are more similar to VHR, PTEN, and KAP.

The most unusual conserved feature of PRLs is the alanine residue following the catalytic arginine. Only two other known phosphatases, CDC25 and the recently identified SKRP1 (35), do not contain a serine or threonine in this position. In CDC25, other serines in the P-loop apparently provide the required hydroxyl functionality because reintroduction of the conserved serine results in a decrease rather than an increase in the catalytic activity (36). In contrast, the active site of PRL-3 does not contain any serines or threonines. Our data clearly show that this is responsible for part of the very low catalytic activity of PRL-3 and suggest that the missing hydroxyl group is provided by the physiological substrate.

The distant positioning of the mobile loop containing the general acid Asp^{72} is another cause of the poor activity toward synthetic substrates. For MKP-3, a phosphatase with a similarly inactive conformation of the general acid loop, a 10^6 increase in the k_{cat}/K_m value was observed when the peptide substrate was replaced by a protein substrate (30). PRL-3 likely undergoes a similar substrate-induced conformational rearrangement to bring Asp^{72} closer to Cys^{104} and enhance catalysis.

The conservation of Cys^{49} in all PRL phosphatases suggests a functional role. There is a growing interest in the oxidation of the catalytic cysteine in phosphatases and its role in the regulation of signaling pathways in response to oxidative stress

(37). Recent data indicate there are two possible mechanisms for the oxidation of the catalytic cysteine side chain that involve its conversion to a sulfenic acid or formation of an intramolecular disulfide bond (38, 39). A plausible role for this disulfide is to protect the catalytic cysteine from irreversible oxidation during oxidative stress. Our results show a potential regulatory role of the conserved Cys^{49} in controlling the efficiency of dephosphorylation under physiological conditions.

Among the other conserved residues in the active site, Phe^{70} likely contributes to the substrate binding/recognition. Two absolutely conserved amino acids, Asn^{142} and Gln^{145}, possibly correspond to invariant glutamines in PTPases (*i.e.* Gln^{262} and Gln^{266} in PTP1B). Gln^{262} in PTP1B is important for phosphoenzyme formation and hydrolysis. In PRL-3, Tyr^{53} is positioned near the active site and could participate in substrate binding, perhaps in a phosphorylation-dependent fashion as observed for Tyr^{138} in the VHR phosphatase (40). The conserved Arg^{47} is sandwiched between Asp^{54} and Asp^{67} and may help define the general acid loop orientation through interactions with Asp^{67} at the beginning of this loop.

On the opposite side of the PRL-3 active site, a conserved cluster of charged amino acids is present. These include Lys^{89}, Glu^{121}, Lys^{125}, Glu^{127}, and a basic stretch of 11 amino acids at the C terminus of the protein in a conserved motif (R/K)*X*(R/K)*X*(R/K)*X*(R/K)*X*(R/K)*X*(R/K), where *X* is an uncharged residue. This basic fragment, located next to the C-terminal prenylation site, likely participates in membrane binding via interactions with phospholipids.

CONCLUSIONS

The PRL-3 structure demonstrates that PRL phosphatases are structurally similar to dual specificity phosphatases. Our structural and mutagenesis studies explain why PRL-3 shows very low enzymatic activity. Absence of a serine/threonine residue in the active site is one reason, because the A111S substitution significantly increases activity. Second, the general acid loop requires a conformational change to bring Asp^{72} closer to the catalytic Cys^{104}. These impediments are likely overcome in the presence of physiological substrates to reveal catalytic activity similar to that observed with other phosphatases. Finally, the redox-dependent disulfide bond between Cys^{49} and the catalytic Cys^{104} may potentially play a regulatory role and deserves further investigation.

Acknowledgments—We thank the Canadian National High Field NMR Centre (NANUC) for assistance and use of the facilities. The technical support of Carine Lievre is appreciated. NRC publication number 46180.

REFERENCES

1. Diamond, R. H., Cressman, D. E., Laz, T. M., Abrams, C. S., and Taub, R. (1994) *Mol. Cell Biol.* **14,** 3752–3762
2. Cates, C. A., Michael, R. L., Stayrook, K. R., Harvey, K. A., Burke, Y. D., Randall, S. K., Crowell, P. L., and Crowell, D. N. (1996) *Cancer Lett.* **110,** 49–55
3. Zeng, Q., Dong, J. M., Guo, K., Li, J., Tan, H. X., Koh, V., Pallen, C. J., Manser, E., and Hong, W. (2003) *Cancer Res.* **63,** 2716–2722
4. Diamond, R. H., Peters, C., Jung, S. P., Greenbaum, L. E., Haber, B. A., Silberg, D. G., Traber, P. G., and Taub, R. (1996) *Am. J. Physiol.* **271,** G121–G129
5. Matter, W. F., Estridge, T., Zhang, C., Belagaje, R., Stancato, L., Dixon, J., Johnson, B., Bloem, L., Pickard, T., Donaghue, M., Acton, S., Jeyaseelan, R., Kadambi, V., and Vlahos, C. J. (2001) *Biochem. Biophys. Res. Commun.* **283,** 1061–1068
6. Zeng, Q., Hong, W., and Tan, Y. H. (1998) *Biochem. Biophys. Res. Commun.* **244,** 421–427
7. Zeng, Q., Si, X., Horstmann, H., Xu, Y., Hong, W., and Pallen, C. J. (2000) *J. Biol. Chem.* **275,** 21444–21452
8. Wang, J., Kirby, C. E., and Herbst, R. (2002) *J. Biol. Chem.* **277,** 46659–46668
9. Zhang, Z. Y. (2002) *Annu. Rev. Pharmacol. Toxicol.* **42,** 209–234
10. Jia, Z., Barford, D., Flint, A. J., and Tonks, N. K. (1995) *Science* **268,** 1754–1758
11. Bardelli, A., Saha, S., Sager, J. A., Romans, K. E., Xin, B., Markowitz, S. D., Lengauer, C., Velculescu, V. E., Kinzler, K. W., and Vogelstein, B. (2003) *Clin. Cancer Res.* **9,** 5607–5615
12. Werner, S. R., Lee, P. A., DeCamp, M. W., Crowell, D. N., Randall, S. K., and Crowell, P. L. (2003) *Cancer Lett.* **202,** 201–211
13. Saha, S., Bardelli, A., Buckhaults, P., Velculescu, V. E., Rago, C., St. Croix, B., Romans, K. E., Choti, M. A., Lengauer, C., Kinzler, K. W., and Vogelstein, B. (2001) *Science* **294,** 1343–1346
14. Kozlov, G., Cheng, J., Lievre, C., Banville, D., Gehring, K., and Ekiel, I. (2002) *J. Biomol. NMR* **24,** 169–170
15. Kuboniwa, H., Grzesiek, S., Delaglio, F., and Bax, A. (1994) *J. Biomol. NMR* **4,** 871–878
16. Pons, J. L., Malliavin, T. E., and Delsuc, M. A. (1997) *J. Biomol. NMR* **8,** 445–452
17. Bartels, C., Xia, T.-H., Billeter, M., Guntert, P., and Wuthrich, K. (1995) *J. Biomol. NMR* **5,** 1–10
18. Cornilescu, G., Delaglio, F., and Bax, A. (1999) *J. Biomol. NMR* **13,** 289–302
19. Nilges, M., Macias, M. J., O'Donoghue, S. I., and Oschkinat, H. (1997) *J. Mol. Biol.* **269,** 408–422
20. Brunger, A. T., Adams, P. D., Clore, G. M., DeLano, W. L., Gros, P., Grosse-Kunstleve, R. W., Jiang, J. S., Kuszewski, J., Nilges, M., Pannu, N. S., Read, R. J., Rice, L. M., Simonson, T., and Warren, G. L. (1998) *Acta Crystallogr. Sect. D Biol. Crystallogr.* **54,** 905–921
21. Laskowski, R. A., Rullmannn, J. A., MacArthur, M. W., Kaptein, R., and Thornton, J. M. (1996) *J. Biomol. NMR* **8,** 477–486
22. Gottlin, E. B., Xu, X., Epstein, D. M., Burke, S. P., Eckstein, J. W., Ballou, D. P., and Dixon, J. E. (1996) *J. Biol. Chem.* **271,** 27445–27449
23. Marti-Renom, M. A., Stuart, A. C., Fiser, A., Sanchez, R., Melo, F., and Sali, A. (2000) *Annu. Rev. Biophys. Biomol. Struct.* **29,** 291–325
24. Cornell, W. D., Cieplak, P., Bayly, C. I., Gould, I. R., Merz, K. M., Jr., Ferguson, D. M., Spellmeyer, D. C., Fox, T., Caldwell, J. W., and Kollman, P. A. (1995) *J. Am. Chem. Soc.* **177,** 5179–5197
25. Lee, J. O., Yang, H., Georgescu, M. M., Di Cristofano, A., Maehama, T., Shi, Y., Dixon, J. E., Pandolfi, P., and Pavletich, N. P. (1999) *Cell* **99,** 323–334
26. Fauman, E. B., Cogswell, J. P., Lovejoy, B., Rocque, W. J., Holmes, W., Montana, V. G., Piwnica-Worms, H., Rink, M. J., and Saper, M. A. (1998) *Cell* **93,** 617–625
27. Song, H., Hanlon, N., Brown, N. R., Noble, M. E., Johnson, L. N., and Barford, D. (2001) *Mol. Cell* **7,** 615–626
28. Yuvaniyama, J., Denu, J. M., Dixon, J. E., and Saper, M. A. (1996) *Science* **272,** 1328–1331
29. Denu, J. M., Zhou, G., Guo, Y., and Dixon, J. E. (1995) *Biochemistry* **34,** 3396–3403
30. Stewart, A. E., Dowd, S., Keyse, S. M., and McDonald, N. Q. (1999) *Nat. Struct. Biol.* **6,** 174–181
31. Denu, J. M., and Dixon, J. E. (1995) *Proc. Natl. Acad. Sci. U. S. A.* **92,** 5910–5914
32. Zhang, Z. Y., Palfey, B. A., Wu, L., and Zhao, Y. (1995) *Biochemistry* **34,** 16389–16396
33. Lee, S. R., Yang, K. S., Kwon, J., Lee, C., Jeong, W., and Rhee, S. G. (2002) *J. Biol. Chem.* **277,** 20336–20342
34. Savitsky, P. A., and Finkel, T. (2002) *J. Biol. Chem.* **277,** 20535–20540
35. Zama, T., Aoki, R., Kamimoto, T., Inoue, K., Ikeda, Y., and Hagiwara, M. (2002) *J. Biol. Chem.* **277,** 23909–23918
36. McCain, D. F., Catrina, I. E., Hengge, A. C., and Zhang, Z. Y. (2002) *J. Biol. Chem.* **277,** 11190–11200
37. Meng, T. C., Fukada, T., and Tonks, N. K. (2002) *Mol. Cell* **9,** 387–399
38. van Montfort, R. L., Congreve, M., Tisi, D., Carr, R., and Jhoti, H. (2003) *Nature* **423,** 773–777
39. Salmeen, A., Andersen, J. N., Myers, M. P., Meng, T. C., Hinks, J. A., Tonks, N. K., and Barford, D. (2003) *Nature* **423,** 769–773
40. Alonso, A., Rahmouni, S., Williams, S., van Stipdonk, M., Jaroszewski, L., Godzik, A., Abraham, R. T., Schoenberger, S. P., and Mustelin, T. (2003) *Nat. Immunol.* **4,** 44–48
41. Kraulis, P. J. (1991) *J. Appl. Crystallogr.* **24,** 946–950
42. Merritt, E. A., and Murphy, M. E. P. (1994) *Acta Crystallogr. Sect. D Biol. Crystallogr.* **50,** 869–873
43. Nicholls, A., Sharp, K. A., and Honig, B. (1991) *Proteins* **11,** 281–296

Structural Insights into Molecular Function of the Metastasis-associated Phosphatase PRL-3

Guennadi Kozlov, Jing Cheng, Edmund Ziomek, Denis Banville, Kalle Gehring and Irena Ekiel

J. Biol. Chem. 2004, 279:11882-11889.
doi: 10.1074/jbc.M312905200 originally published online January 1, 2004
